Electronic Supplementary Material (ESI) for Inorganic Chemistry Frontiers.

Supplemental Material

$Sb/SbPO_4$@3D-G Composite as a Promising Anode Material for Sodium-Ion Batteries

Tingzhen Xie†[a], Zhigang Zhang†[a], Xiaoping Lin†[a], Yidong Shen†[a], Qiuhong Li*†[a]

a Pen-Tung Sah Institute of Micro-Nano Science and Technology, Xiamen University, Xiamen 361005, China.

*Corresponding author.
E-mail address: liqiuhong@xmu.edu.cn

Supplemental Information consists of one table and eight figures over eleven pages. Figure S1 is about photo of Sb_2O_3@3D-G，Figure S2 is about XRD patterns of Sb_2O_3, Figure S3 and Figure S5 are about SEM images of $Sb/SbPO_4$@3D-G, Figure S4 is about BET result，Figure S6 is about long cycle performance of SSPG-M, Figure S7 is about SEM images of $Sb/SbPO_4$@3D-G after cycles. Figure S8 is about the cycling performance comparison, and the Table S1 is about comparison of the electrochemical performance of Sb-based materials for SIBs.

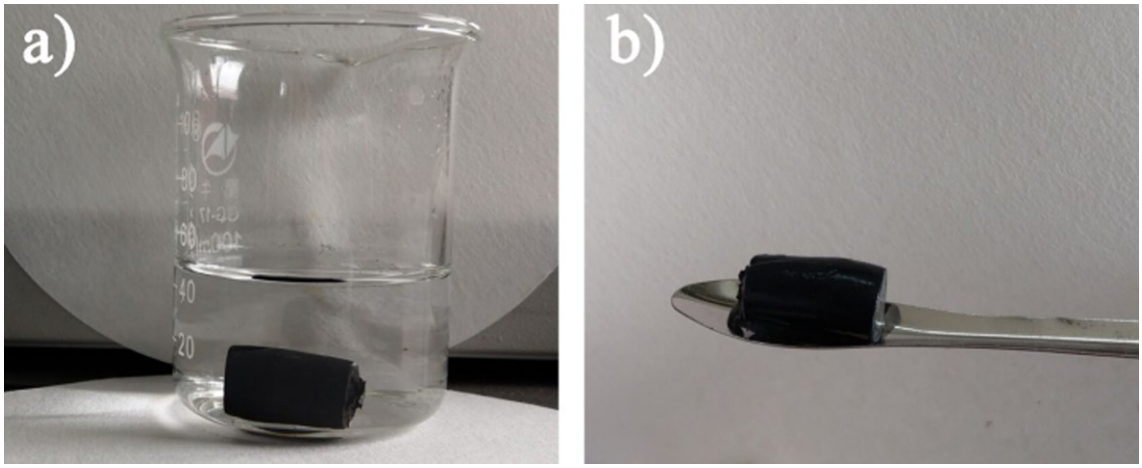

Fig. S1. The photo of black hydrogel Sb_2O_3@3D-G.

Fig. S1 displays the photo of Sb_2O_3@3D-G. The product is a black hydrogel and elastic with dense structure.

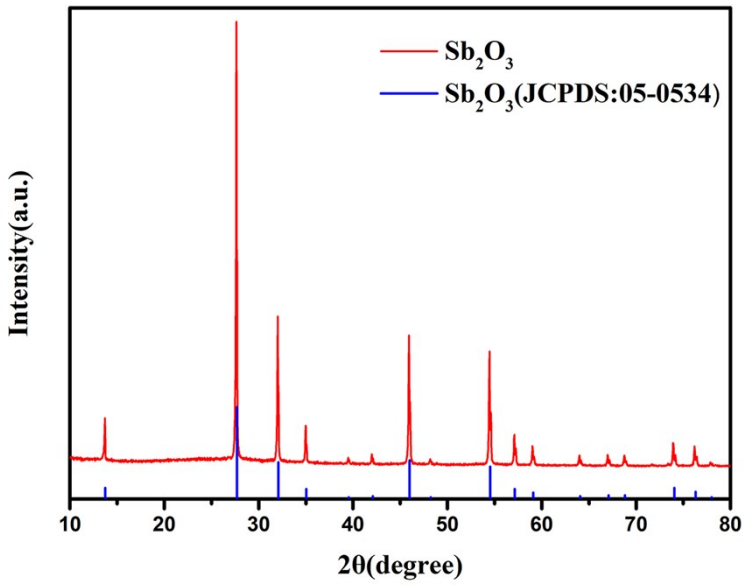

Fig. S2. XRD pattern of Sb_2O_3.

Fig. S2 shows the XRD pattern of Sb_2O_3. It is evident that all the diffraction peaks are in good accordance with the corresponding crystal planes of cubic Sb_2O_3 (JCPDS No.05-0534).

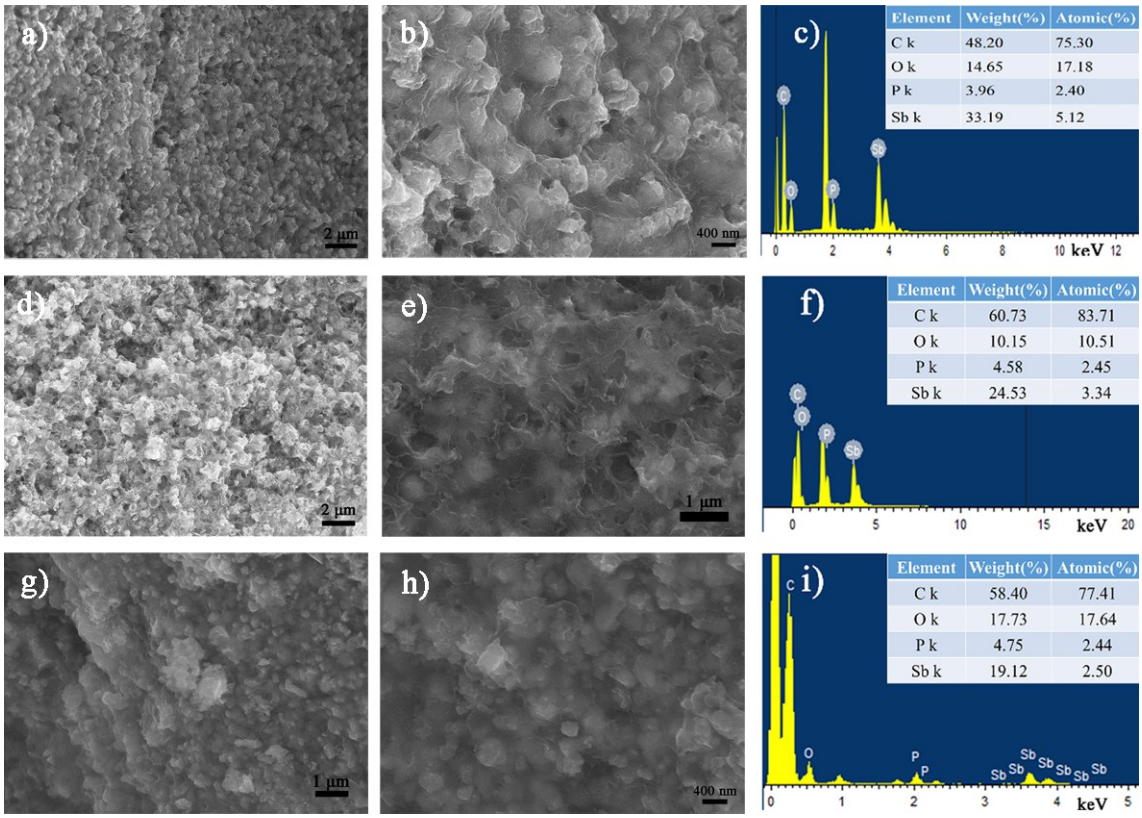

Fig. S3. SEM images and EDS spectrum of a-c) SSPG-M; d-f) SSPG-L; and g-i) $SbPO_4$@3D-G.

Fig. S3 shows SEM images and EDS spectrum of SSPG-M, SSPG-L and $SbPO_4$@3D-G. There are no distinct differences in morphology of three samples. The EDS results are accordant with the element ratios in relevant products.

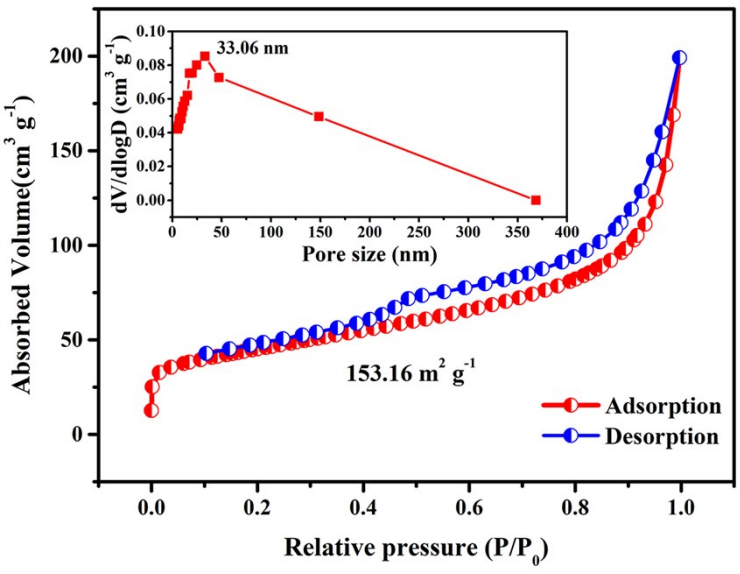

Fig. S4. Nitrogen adsorption-desorption isotherm and pore size distribution of SSPG-M.

Fig. S4 shows the nitrogen adsorption-desorption isotherm and pore size distribution of SSPG-M. The specific surface area was calculated according to the Brunauer-Emmett-Teller (BET) method and the pore size distribution was analyzed by Barrett-Joyner-Halenda (BJH) method. The SSPG-M sample shows an IV-type adsorption-desorption isothermal curve, and the specific surface area is about 153.16 m^2 g^{-1}.

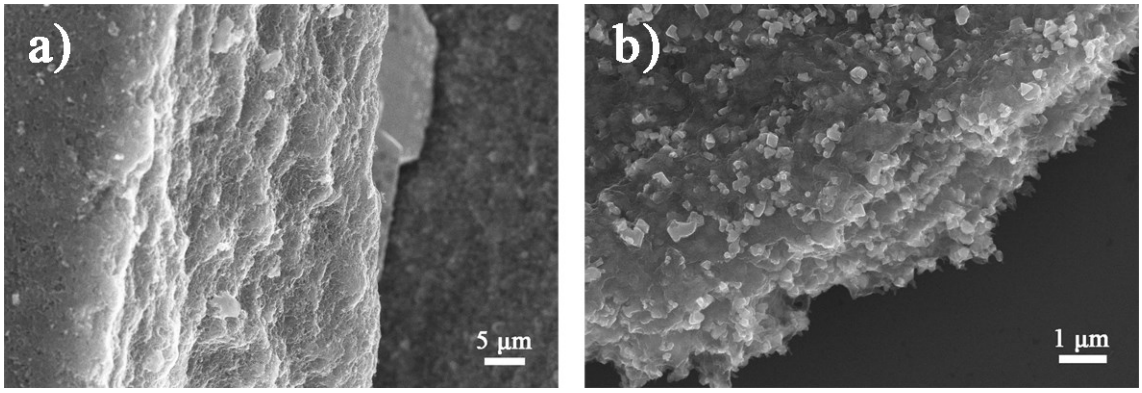

Fig. S5. The lateral morphology of Sb/$SbPO_4$@3D-G: a) in whole; b) in partial.

Fig. S5 shows the lateral morphology of Sb/$SbPO_4$@3D-G. It is clear that the graphene layers are stacked layer by layer.

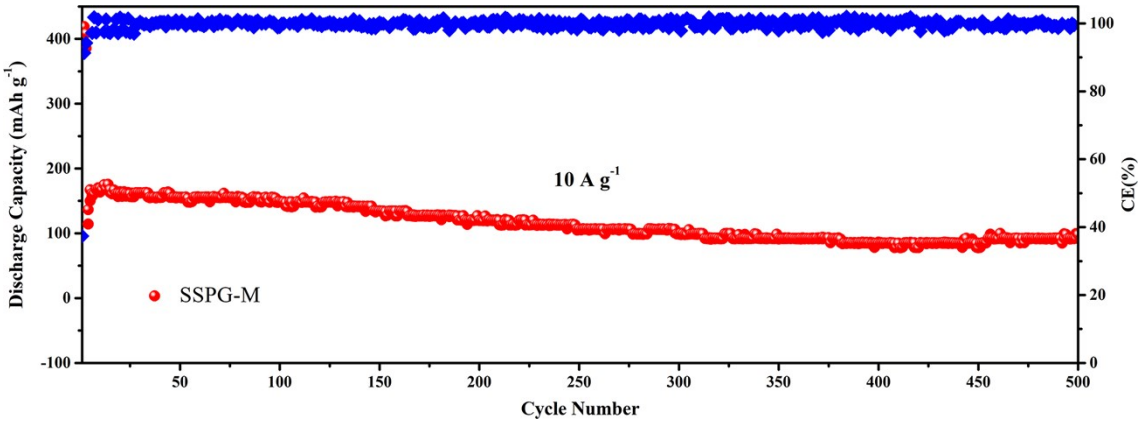

Fig. S6. Cycling performance of SSPG-M at 10 A g^{-1} between 0.01-1.5 V.

Fig. S6 exhibits the long cycle performance of SSPG-M at 10 A g^{-1} between 0.01 and 1.5 V. We can observe that the capacity still remains 98 mA h g^{-1} after 500 cycles. Besides, the coulombic efficiency is stabilized around 100% all along.

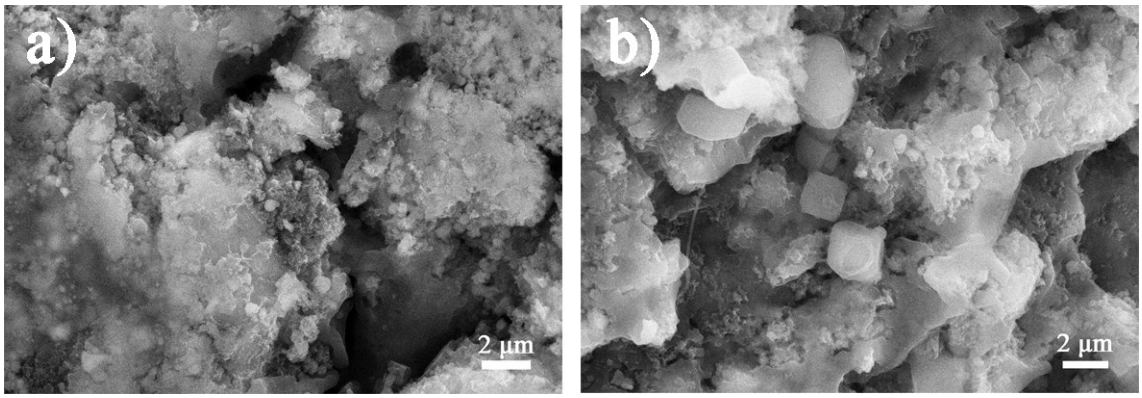

Fig. S7. a-b) SEM images of Sb/$SbPO_4$@3D-G electrode after 100 cycles at 0.1 A g^{-1}.

Fig. S7 shows the SEM images of Sb/$SbPO_4$@3D-G electrode after 100 cycles at 0.1 A g^{-1}. It can be seen that the octahedron morphology of nanoparticles could be well maintained after 100 cycles, although experiencing inevitable volume expansion.

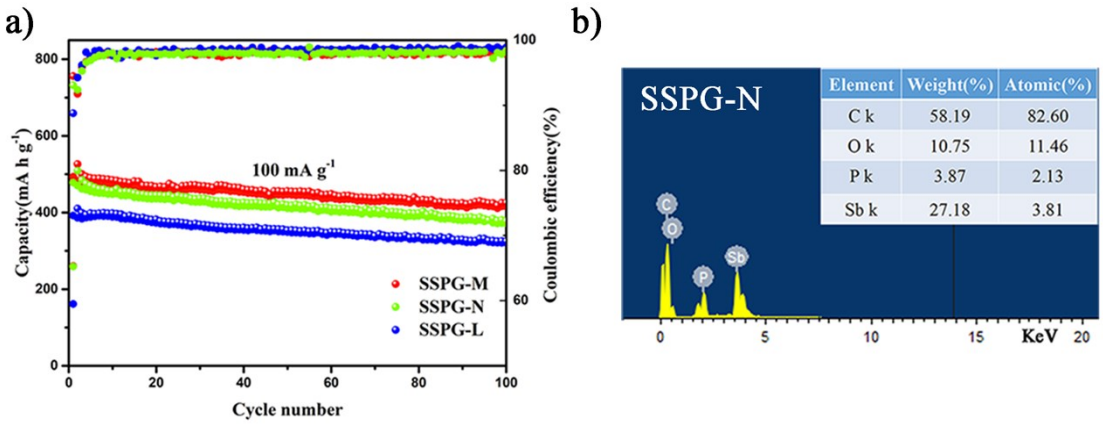

Fig. S8. a) Cycling performance of SSPG-M、SSPG-N、SSPG-L electrodes at 100 mA g^{-1}; b) EDS spectrum of SSPG-N sample.

Fig. S8 deeply discusses the issue that more content of Sb can provide more capacity and higher initial coulombic efficiency. The contents of elements in SSPG-N is shown in Fig. S8b. It is obvious that the capacity gets promoted as the content of Sb in the sample increased in Fig. S8a. Moreover, more content of Sb can also provide higher initial coulombic efficiency.

Table S1 Comparison of the electrochemical performance of Sb-based materials for SIBs.

Materials	Shape	Remaining capacity (mA h g^{-1})	Rate capability (mA h g^{-1})	Ref.
$Sb_{47}Fe_{39}P_{14}$	fiber-like structure	422mA h g^{-1} @0.1A g^{-1} after 200 cycles	441.7—245.8—477.5 (0.1—2—0.1 A g^{-1})	1
Sb_2S_3/carbon–silicon oxide	nanofibers	321mA h g^{-1} @0.2A g^{-1} after 200 cycles	532—221— ~480 (0.1—5—0.1 A g^{-1})	2
Sb_2Se_3/C	amorphous	378mA h g^{-1} @0.05A g^{-1} after 50 cycles	270mA h g^{-1} @1.2 A g^{-1}	3
Sb-C	rod-like	430.9mA h g^{-1} @0.1A g^{-1} after 100 cycles	499.8—259.1—405.6 (0.05—2.5—0.05 A g^{-1})	4
Sb/N-doped porous carbon	1D structure	400.9mA h g^{-1} @0.1A g^{-1} after 100 cycles	502.9—50.4—421.8 (0.05—5—0.05 A g^{-1})	5
$SbPO_4$/rGO	layered structure	280mA h g^{-1} @0.5A g^{-1} after 100 cycles	323—214— ~320 (0.1—5—0.1 A g^{-1})	6
Sb@TiO_{2-X}	nanoplates	540mA h g^{-1} @0.1A g^{-1} after 100 cycles	571—429—562 (0.1—3.2—0.1 A g^{-1})	7
SnS/SnSb@C	nanofibers	270mA h g^{-1} @0.2A g^{-1} after 200 cycles	458—159—425 (0.05—2—0.05 A g^{-1})	8
Sb/$SbPO_4$@3D-G	3D structure	425.3mA h g^{-1} @0.1A g^{-1} after 100 cycles	484.4—236.1—459.4 (0.05—5—0.05 A g^{-1})	This work

References

1. W. Rong, J. You, X. Zheng, G. Tu, S. Tao, P. Zhang, Y. Wang and J. Li, Electrodeposited binder-free antimony iron phosphorous composites as advanced anodes for sodium-ion batteries, *ChemElectroChem*, 2019, **6**, 5420-5427.
2. J. Xie, J. Xia, Y. Yuan, L. Liu, Y. Zhang, S. Nie, H. Yan and X. Wang, Sb_2S_3 embedded in carbon–silicon oxide nanofibers as high-performance anode materials for lithium-ion and sodium-ion batteries, *J. Power Sources*, 2019, **435**, 226762.
3. K. Nam and C. Park, 2D layered Sb2Se3-based amorphous composite for high-performance Li and Na-ion battery anodes, *J. Power Source*s, 2019, **433**, 126639.
4. L. Fan, J. Zhang, J. Cui, Y. Zhu, J. Liang, L.Wang and Y. Qian, Electrochemical performance of rod-like Sb–C composite as anodes for Li-ion and Na-ion batteries, *J. Mater. Chem. A*., 2015, **3**, 3276-3280.
5. Q. Yang, J. Zhou, G. Zhang, C. Guo, M. Li, Y. Zhu and Y. Qian, Sb nanoparticles uniformly dispersed in 1-D N doped porous carbon as anodes for Li-ion and Na-ion batteries, *J. Mater. Chem. A*., 2017, **5**, 12144-12148.
6. J. Pan, S. Chen, Q. Fu, Y. Sun, Y. Zhang, N. Lin, P. Gao, J. Yang and Y. Qian, Layered-structure $SbPO_4$/reduced graphene oxide: An advanced anode material for sodium ion batteries, *ACS Nano*, 2018, **12**, 12869-12878.
7. P. Li, X. Guo, S. Wang, R. Zang, X. Li, Z. Man, P. Li, S. Liu, Y. Wu and G. Wang, Two-dimensional Sb@TiO_{2-x} nanoplates as a high performance anode material for sodium-ion batteries, *J. Mater. Chem. A*., 2019, **7**, 2553-2559.
8. J. Zhu, C. Shang, Z. Wang, J. Zhang, Y. Liu, S. Gu, L. Zhou, H. Cheng, Y. Gu and Z. Lu, SnS/SnSb@C nanofibers with enhanced cycling stability via vulcanization as an anode for sodium-ion batteries, *ChemElectroChem*, 2018, **5**, 1098-1104.